Int. J. Electrochem. Sci., 17 **(2022)** Article Number: 22099, doi: 10.20964/2022.09.08

International Journal of
ELECTROCHEMICAL
SCIENCE
www.electrochemsci.org

Electrochemical Corrosion Characteristics of 316L Stainless Steel in Simulated Coastal Gold Mine Wastewater under Different pH

Liyi Zhu[1], *Peng Yang*[1,2,*], *Wensheng Lyu*[1], *Qixuan Wang*[3], *Kun Wang*[4]

[1] School of Civil and Resource Engineering, University of Science and Technology Beijing, Beijing 100083, China
[2] Beijing Key Laboratory of Information Service Engineering, Beijing Union University, Beijing 100101, China
[3] State Key Laboratory of Safety Technology for Metal Mines, Changsha Institute of Mining Research Co. Ltd., Changsha 410012, China
[4] College of Energy and Mining Engineering, Shandong University of Science and Technology, Qingdao 266590, China
[*]E-mail: yangpeng@buu.edu.cn

Received: 6 April 2022 / *Accepted:* 23 May 2022 / *Published:* 7 August 2022

The passivation behavior of 316L stainless steel in media simulating acidic coastal mine water solution (ACMW) with pH 4 and coastal mine water (CMW) with pH 7 was evaluated by open-circuit potential, potentiodynamic polarization behaviour and electrochemical impedance spectroscopy (EIS). Scanning electron microscope (SEM) was used to observe and analyze the morphological characteristics of the immersion samples. The open-circuit potential profiles and polarisation curves suggest that the passive film can be formed on 316L stainless steel surface after immersion in ACMW for 7 days, while it takes 30 days to form a stable passivation film in CMW. The corrosion state changed from spontaneous passivation to pitting after immersion in two solutions for about 4 months. During long-term immersion, pitting is controlled by charge transfer and diffusion processes. The corrosion potential and pitting potential of 316L stainless steel in CMW are higher than those in ACMW. Electrochemical impedance spectroscopy confirms that 316L stainless steel has good passivation performance in CMW, and stainless steel is more easily corroded in ACMW. The SEM images further prove that the conclusion of electrochemical test is correct.

Keywords: Stainless steel, Seashore mine solution, Polarization, EIS, SEM, Pitting corrosion

1. INTRODUCTION

Metal mineral resources are the fundamental sources of metal products and materials, and play a

significant role in promoting the development and progress of social economy. With the continuous depletion of shallow resources, human beings are gradually mining mineral resources in the deep strata, including the ocean. At present, sulfide is a high proportion of minerals in China's metal mining, accounting for about 75% of all kinds of minerals[1], especially copper, lead, zinc and other non-ferrous heavy metal deposits[2]. In addition, China's metal mines have some obvious characteristics, such as more lean ore, less rich ore, less single ore, complex mineral symbiosis and associated relationship, fine disseminated particle size of useful minerals, low metal grade, large mineral stripping ratio and so on. Thus, a large amount of mine solid waste is produced during mining. In non-ferrous metal sulfide mines, about 1.25 tons of waste rock will be produced for each ton of ore mined, and about 0.92 tons of tailings will be produced for each ton of ore extracted. Only about 18.9% of the tailings are used for goaf filling and building material recycling, and the rest are basically stored in tailings pond[3].

A large number of tailings and waste rocks are exposed to the air, and then the sulfur and sulfide in tailings and waste rocks are oxidized to form acid mine wastewater containing sulfuric acid and sulfate through the leaching of atmospheric rainfall and the catalysis of thiobacillus thiooxidans, thiobacillus ferrooxidans and other microorganisms[4-6]. The pH value of acid mine wastewater is generally low, in addition, it also contains a certain amount of copper, zinc, lead, manganese and other elements. Due to the low pH value and containing many heavy metal ions, it will not only pollute the soil, acidify the soil and kill plants, but also cause corrosion of water pumps, mine pipelines, mine equipment and some monitoring instruments and sensors, resulting in equipment damage[7].

The solid minerals such as waste rock and tailing produced in the process of mining and extracting of some deposits hosted in the seabed or coastal zone are often rich in chloride and sulfate. Similarly, under the action of external environment and microbial catalysis, high concentration of strong acid brine will be formed.

Tailings pond formed by tailings storage not only occupies a large amount of land, but also is a major hazard source with high potential energy. Once the construction and operation of tailings pond are lack of safety control, it is prone to dam failure, causing immeasurable casualties and economic losses[8]. In the daily operation of tailings pond, online monitoring is needed, such as saturation line monitoring, reservoir water level monitoring, dam displacement monitoring, etc. The monitoring of these parameters needs to be realized by embedding a large number of instruments and sensors in the tailings pond. Some tailing ponds are located in the seaside, because of their unique and complex chemical environment, monitoring instruments and sensors are easy to be corroded. Due to the good corrosion resistance of 316L stainless steel in common water and chemical environment, the corrosion of 316L stainless steel has been widely reported in the past two or three decades. The corrosion characteristics of 316L stainless steel were studied based on different corrosion media such as seawater, concrete[9], sludge[10], high temperature pressurized water[11] and oilfield brine[12]. In contrast, fewer papers can find the research on the corrosion resistance of 316L stainless steel in the strong acid mine water environment of seaside mine for a long time.

Therefore, the corrosion process of 316L stainless steel in mine water with pH 4 and 7 was monitored by open-circuit potential method, potentiodynamic polarization method, electrochemical impedance spectroscopy and scanning electron microscope (SEM) for one year. The main purposes are to gain the electrochemical corrosion characteristics of 316 L stainless steel in coastal mine water

environment, and provide basic information for the material selection and safe operation of monitoring instruments and sensors in tailings pond.

2. EXPERIMENTAL

2.1 Material and solution

316L austenitic stainless steel, which is commonly used as the shell material of monitoring instruments in tailings ponds, was used in the experiments. It is an austenitic ultra-low carbon steel with the main chemical components (wt.%): 0.019 C, 0.7 Si, 1.4 Mn, 0.031 P, 0.018 S, 16.77 Cr, 10.76 Ni, 2.79 Mo, and Fe balance. The rectangular specimen for immersion test was suspended in a solution with an exposed area of about 30 cm^2. The working surface was abraded with SiC papers of grit size from 120# to 1000# and cleaned with alcohol and distilled water.

The coastal mine water(CMW) was taken from Xincheng Gold Mine of Shandong Gold Group, China, which is located at the seaside. The pH of the mine water was measured by pH meter to be 7. In addition, in order to simulate the acid mine water produced in some coastal mines with sulfide, the acidic coastal mine water solution(ACMW) with pH of 4 was prepared by using analytically pure sulfuric acid and the mine water of Xincheng Gold Mine. In order to analyze the components and contents of brine in two kinds of corrosion solutions, ion concentration analysis was performed on the corrosion solutions. Ions such as Na^+, K^+, Mg^{2+}, Ca^{2+} and anions such as Cl^-, SO_4^{2-}, NO_3^- were determined by Dionex AQUION ICS-2100 ion chromatography analyzer (Thermo-Fisher, USA), and the results are shown in Table 1. It can be seen from Table 1 that the ACMW contains a lot of halide ions and the concentration was significantly higher, especially the concentration of Cl^- reached 17226.5 mg/L, and the concentration of SO_4^{2-} reached 4273.3 mg/L. Similarly, the CMW also contained a large amount of halide ions and the concentration was significantly higher, especially the concentration of Cl^- reached 14581.9 mg/L, and the concentration of SO_4^{2-} reached 2536.2 mg/L. The Cl^- concentration in the two corrosion simulation solutions was relatively high and basically close to each other.

Table 1. Ion concentration of corrosion simulation solution with pH=4 and 7 (mg/L)

Corrosive solution	pH	Na^+	K^+	Ca^{2+}	Mg^{2+}	Cl^-	SO_4^{2-}	NO_3^-
Acidic coastal mine water	4	11788.4	385.4	736.4	1516.2	17226.5	4273.3	35.6
Coastal mine water	7	9354.6	324.8	1214.6	1351.5	14581.9	2536.2	39.2

2.2 Electrochemical measurements

The electrochemical test was performed by Versa STAT 3 electrochemical workstation (Princeton Applied Research, USA). In the experiment, a classic three-electrode cell was used for electrochemical measurements. The corrosion sample was used as the working electrode, the saturated calomel electrode

(SCE) was used as the reference electrode, and the platinum sheet was used as the auxiliary electrode. After different times of immersion in solution with different pH, The EIS measurements were carried out at the corrosion potential in the frequency range from 100 kHz to 10 mHz with a voltage amplitude of 10 mV (rms). ZSimpWin software was used to fit impedance spectrum. The potentiodynamic polarization was measured in the scanning range of -300 ~2000 mV (relative to the open-circuit potential vs.OCP) and the scanning rate was 0.5 mV/s, and the data of polarization curve was fitted by Tafel formula in E-Clab software. It is worth noting that all electrochemical experiments were carried out after the sample was soaked, and the test was the soaked solution.

2.3 Immersion test

The test solutions were acidic coastal mine water simulation solution (pH=4) and coastal mine water (pH=7). The immersion test time was divided into seven cycles: 0 day (0 d), 7 days (7 d) 15 days (15 d), 30 days (30 d), 2 months (2 m), 4 months (4 m), and 12 months (12 m). Therefore, according to the type of test solution, there were two large groups, and then each solution was subdivided into seven groups according to the immersion times. Fourteen beakers were prepared, each of which contained one test solution. Each beaker contained 1000 ml solution at 20 ℃. Two rectangular samples (one for electrochemical test and the other for surface morphology analysis) were suspended in each beaker. The upper part of the beaker was sealed with plastic film to prevent evaporation of the test solution. The test solution was renewed once a month. According to the immersion test cycle, samples are taken one by one regularly. After taking out the solution, each sample was washed with cotton and dilute nitric acid solution to remove the deposited salt film. The development of pitting corrosion after immersion was analyzed.

2.4 Surface analysis

In order to analyze the surface morphology and pitting corrosion of samples immersed in different test solutions, the samples were observed by Geminism500 scanning electron microscope (ZEISS, Germany).

3. RESULTS AND DISCUSSION

3.1 Electrochemical measurements

3.1.1 Open-circuit potential

The OCP transients, as an important parameter to evaluate the tendency to corrosion [13]. Fig. 1 shows the variation of OCP for 316L stainless steel in different solutions for different days of immersion. From the beginning of the experiment to about 250 s, the OCP was unstable, and each curve had an upward or downward trend. With the increase of test time, the OCP of each curve gradually tended to be

stable. It can be seen from Fig. 1 (a) that the OPC of stainless steel sample was about - 270 ~ 110 mV in each immersion period. When the potential of the stainless steel sample at the beginning (immersion time = 0 d) tended to be stable, the value was about - 270 mV. When the immersion time was 7 d, the OPC reached the peak value, which was about 110 mV. It can be seen from Fig. 1(b) that the OCP in each immersion period was approximately -170~60 mV. The OCP at the beginning (immersion time = 0 d) was about -110 mV. The OCP remained positive during the immersion period of 0~30 d, and the maximum value was about 60 mV when the immersion period was 30 d, at which time the corrosion tendency of samples was the least significant. The OCP value becomes higher, indicating that a more stable passive film was formed under the interaction of surface and electrolyte in the medium[14]. When the immersion time continued to increase, the OCP curve shifts negatively again, and decreases. After immersion for 12 m, the OCP was about -170 mV, and the corrosion tendency of the sample was most obvious. The decrease of OCP was also attributed to the thinning of passivation film or the formation of less dense passivation film[9, 15, 16].

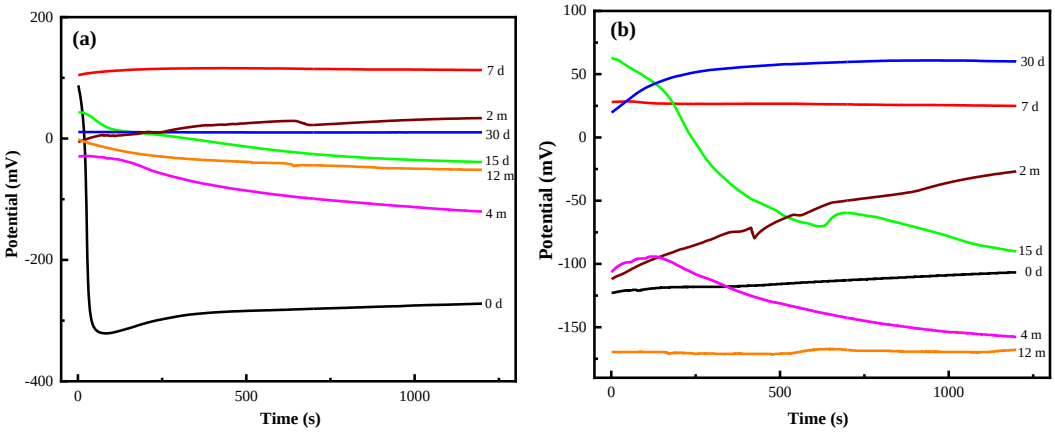

Figure 1. Variation of open-circuit potential with time for the specimen immersed in two test solutions: (a) pH = 4, (b) pH = 7.

3.1.2 Potentiodynamic polarization behavior

In order to further investigate the passivation properties of 316L stainless steel in two kind of corrosive solutions, the potentiodynamic polarization measurements were carried out for different days of immersion. The potentiodynamic polarization curves of 316L stainless steel after immersing in ACMW and CMW for different times are presented in Fig. 2. In general, the polarization curves were very similar, because the passive zone with almost constant current density could be observed. There was a sharp increase in current density caused by the beginning of pitting in the curve, indicating that the kinetics of the corrosion process was basically the same. The corrosion potential (E_{corr}), corrosion current density (i_{corr}) and pitting potential (E_{pit}) obtained from polarization curves of 316L stainless steel in different pH solutions are summarized in Table 2.

As shown in Fig. 2 and Table 2, the variation trend of E_{corr} after immersion in ACMW was

interesting. The E_{corr} of the sample at the beginning (immersion time = 0 d) was the lowest, which increased with the immersion time and reached the maximum value of 25 mV at 7 days. With the immersion time prolonged, the E_{corr} decreased, and there was no significant difference between the two E_{corr} after 15 days and 30 days of immersion. However, the E_{corr} increased after 2 months of immersion, decreased after 4 months of immersion, and decreased to - 296 mV after 12 months of immersion. This shows that passive film will be formed on the stainless steel surface in ACMW in a short period of time, and the E_{corr} will increase rapidly at the beginning.

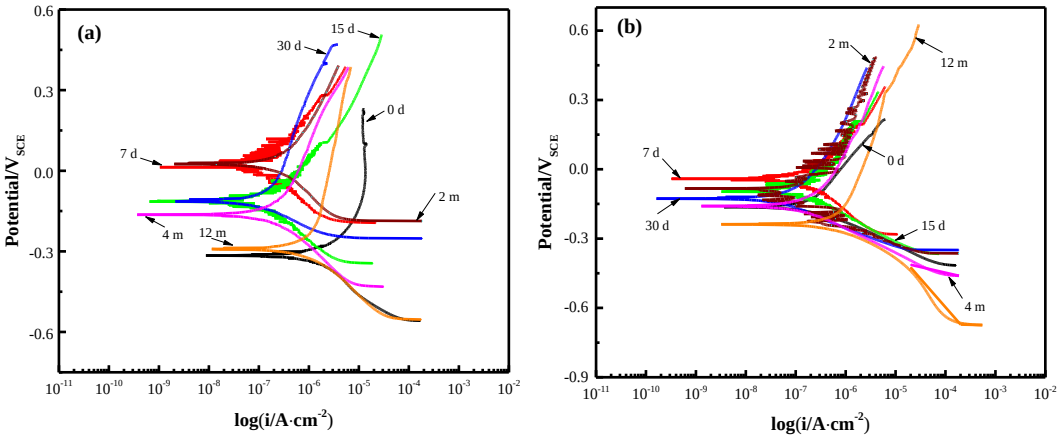

Figure 2. The potentiodynamic polarization curves of stainless steel immersed in different solutions for different days: (a) pH = 4, (b) pH = 7.

Table 2. Electrochemical parameters derived from the polarization curves of samples with different immersion periods in different simulated solutions

	Immersion periods	E_{corr} (mV vs.V_{SCE})	i_{corr} (μA·cm^{-2})	E_{pit} (mV vs.V_{SCE})
pH=4	0 d	-335	1.925	252
	7 d	25	0.030	393
	15 d	-124	0.022	515
	30 d	-118	0.158	530
	2 m	29	0.087	426
	4 m	-163	0.168	404
	12 m	-296	0.862	485
pH=7	0 d	-164	0.102	221
	7 d	-47	0.109	548
	15 d	-83	0.124	356
	30 d	-135	0.036	479
	2 m	-78	0.075	553
	4 m	-174	0.177	454
	12 m	-242	0.715	533

However, with the increase of immersion time, the passivation film was dissolved, and the

potential decreased rapidly. After a period of time, the passivation film grew again, and then was dissolved until pitting corrosion occurred. The variation of passive film was consistent with the results observed by other researchers[17, 18]. The pitting corrosion occurred for 4 months. It should be noted that the variation range of corrosion potential was small after immersion in CMW for different days. The variation trend of E_{corr} was similar to that of stainless steel immersed in ACMW, and pitting corrosion also occurs after 4 months of immersion. However, the E_{corr} immersed in neutral solution reached the maximum after 30 days, while that in acidic solution only took 7 days. In addition, it can be found that the range of E_{corr} in neutral solution was obviously smaller than that in acid solution. Furthermore, the E_{pit} of stainless steel immersed in CMW was generally higher than that immersed in ACMW, which indicated that 316L stainless steel was more easily corroded in ACMW than in CMW.

3.1.3 Electrochemical impedance spectroscopy

Aiming at a better understanding of the growth and physical differences between the passivating films formed, EIS experiments were carried out under different immersion time. Fig. 4 and Fig. 5 respectively show representative EIS diagrams for both simulated solutions at different immersion days. The Nyquist diagram in Fig. 4 (a) shows that in the ACMW, the diameter of the capacitive loop increased initially followed by a decrease with time, but then again increased and decreased finally, which was similar to the variation of corrosion potential in the potentiodynamic polarization experiment. The increase of the diameter of the capacitive loop was a typical aspect observed when the sample surface becomes more oxidized, which confirms that the passivation process was taking place. The decrease of capacitive loop diameter indicated that the passive film was dissolving until pitting occurred. The variation trend of the diameter of the capacitive loop in the Nyquist diagram of Fig. 5 (a) was also similar to that of the corrosion potential in the potentiodynamic polarization experiment. The Bode diagram in Fig. 4 (b) shows that the highest phase angle of 316L stainless steel soaked for 7 d, 30 d and 2 m was more than 80 °. It shows that a stable passive film was formed on the surface of stainless steel at this time, which further proved the conclusion of potentiodynamic polarization test. The closer the maximum phase angle is to 90°, the more complete the passivation film, and the smaller the integrity, the worse the integrity, as described at Wang et al. [19] Compared with Bode diagram in Fig. 5 (b), the maximum phase angle of stainless steel after immersion in CMW for different times was generally larger than that in ACMW. It was also confirmed that 316L stainless steel obtained from potentiodynamic polarization experiment was more likely to be corroded in ACMW than in CMW.

Different equivalent circuit models have been used to interpret the impedance spectra of passive and active metal surfaces[20-28]. Therefore, due to the electrochemical reaction between passivation film and metal/film interface formed on the stainless steel surface, the equivalent circuit shown in Fig.6, was most suitable for explaining the physical phenomena represented by experimental data[29-31], as shown in the fitting curve in Fig. 4, and the fitting values are shown in Table 3 and 4. The high frequency time constant is represented by the solution resistance (R_{sol}) and the passive layer resistance (R_{film}) with constant phase element (CPE) associated with the passive film capacitor (Q_{film}). The low frequency time constant is expressed by charge transfer resistance (R_{ct}) and electric double layer capacitance (Q_{dl}). Note

that in the equivalent circuit, CPE was used instead of pure capacitor to consider the inhomogeneity of the enhanced/simulated pore solution interface [28, 32, 33]. In addition, this analysis of the proposed circuit produces fitting data with absolute error less than 10%.

From Table 3 and 4, the charge transfer resistance and passive layer resistance of 316L stainless steel in CMW are higher than those in ACMW. This more complete analysis further confirmed that the film obtained in CMW has better passivation performance than that obtained in ACMW.

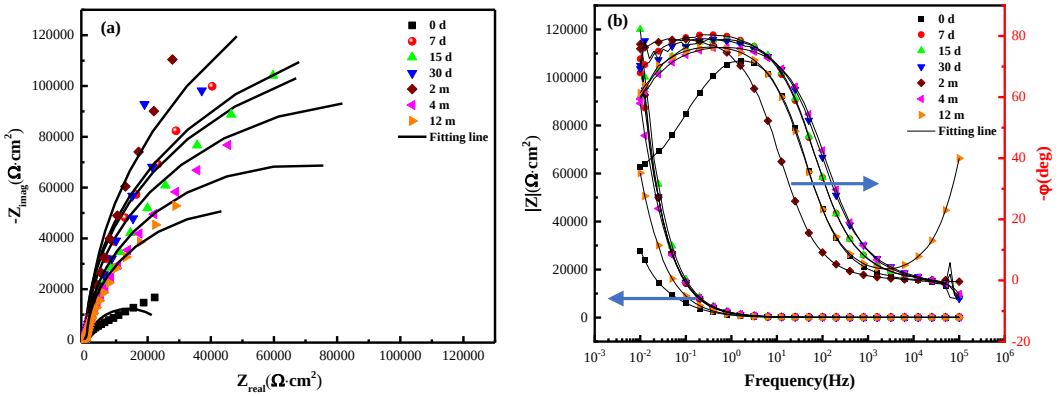

Figure 4. EIS of the steels in test solution with pH 4 at different immersion time:(a) Nyquist plot, (b) Bode plot.

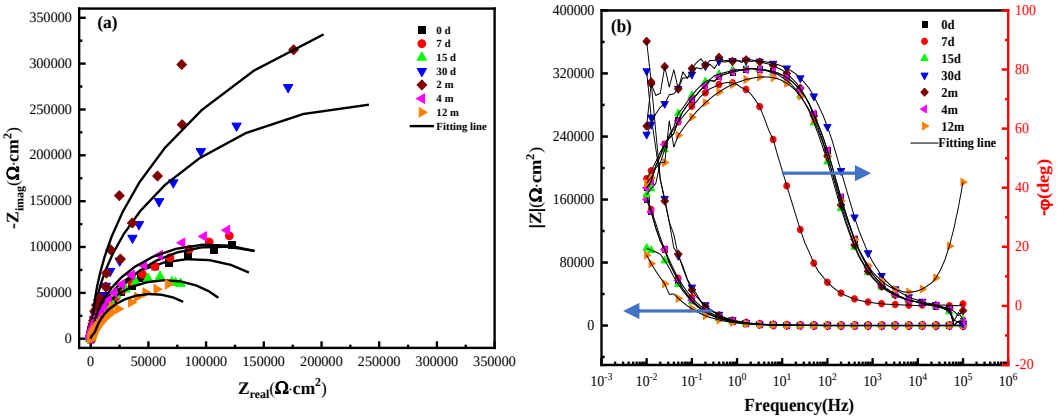

Figure 5. EIS of the steels in test solution with pH 7 at different immersion time: (a) Nyquist plot, (b) Bode plot.

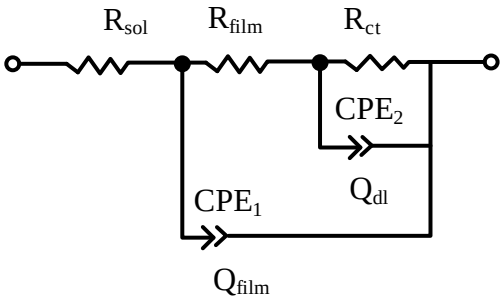

Figure 6. Equivalent electrical circuits proposed to fit impedance spectra

Table 3. EIS fitting results of 316L stainless steel samples with different immersion time in ACMW

Immersion periods	R_{sol} ($\Omega \cdot cm^2$)	Q_{film} ($\Omega^{-1} \cdot cm^{-2} \cdot s^{-n}$)	R_{film} ($\Omega \cdot cm^2$)	Q_{dl} ($\Omega^{-1} \cdot cm^{-2} \cdot s^{-n}$)	R_{ct} ($\Omega \cdot cm^2$)
0 d	42.4	1.22×10^{-4}	4.13×10^{3}	2.42×10^{-4}	2.25×10^{4}
7 d	41.0	6.08×10^{-5}	1.77×10^{3}	4.90×10^{-5}	2.27×10^{5}
15 d	45.7	5.52×10^{-5}	2.78×10^{3}	4.39×10^{-5}	1.91×10^{5}
30 d	33.4	5.36×10^{-5}	1.68×10^{3}	5.29×10^{-5}	2.46×10^{5}
2 m	217.0	6.78×10^{-5}	5.80×10^{3}	4.89×10^{-5}	3.51×10^{5}
4 m	34.8	4.83×10^{-5}	2.51×10^{3}	5.85×10^{-5}	1.42×10^{5}
12 m	56.2	9.54×10^{-5}	3.02×10^{3}	9.22×10^{-5}	1.08×10^{5}

Table 4. EIS fitting results of 316L stainless steel samples with different immersion time in CMW

Immersion periods	R_{sol} ($\Omega \cdot cm^2$)	Q_{film} ($\Omega^{-1} \cdot cm^{-2} \cdot s^{-n}$)	R_{film} ($\Omega \cdot cm^2$)	Q_{dl} ($\Omega^{-1} \cdot cm^{-2} \cdot s^{-n}$)	R_{ct} ($\Omega \cdot cm^2$)
0 d	42.4	1.22×10^{-4}	4.13×10^{3}	2.42×10^{-4}	2.25×10^{4}
7 d	494.0	3.07×10^{-5}	4.35×10^{4}	3.61×10^{-5}	1.69×10^{5}
15 d	45.2	3.09×10^{-5}	7.92×10^{3}	2.33×10^{-5}	1.24×10^{5}
30 d	36.8	2.25×10^{-5}	1.53×10^{4}	1.22×10^{-5}	5.01×10^{5}
2 m	49.2	2.55×10^{-5}	1.49×10^{4}	1.04×10^{-5}	7.43×10^{5}
4 m	40.2	3.13×10^{-5}	1.08×10^{4}	2.38×10^{-5}	1.99×10^{5}
12 m	49.2	3.69×10^{-5}	1.25×10^{4}	5.57×10^{-5}	9.06×10^{4}

3.2. 316L stainless steel morphological characterization

In order to verify the results of potentiodynamic polarization experiment and EIS experiment, the morphology of the working electrode surface was studied by scanning electron microscope (SEM) after immersion in ACMW and CMW. Figs. 6, 7, 8 nd 9 are representative micrographs of surface changes of 316L stainless steel after immersion in two solutions for 0 d, 7 d, 4 d and 12 m respectively. Note that the scratch in the picture is a defect formed in the polishing process, which does not affect the experimental results. It can be seen from Fig. 6 that the surface of the stainless steel sample that has not been immersed is flat without pits. It can be seen from Fig. 7 that after continuous immersion in two solutions for 7 d, no pits were found on the surface of the sample. From the scratch depth formed in the polishing process, the scratch became shallow obviously in Fig. 7, which indicates that the passive film was formed on the surface of stainless steel. According to Pourbaix diagram[34], it is reasonable that the growth of thin films is due to the formation of iron (hydrogen) oxides. According to the literatures[35, 36], the corrosion products on steel contain both FeOOH and Fe_2O_3. The anodic process is characterized

by iron dissolution [28, 37, 38]:

$$Fe \rightarrow Fe^{2+} + 2e^{-} \quad (1)$$

Fe $(OH)_2$ corrosion scale is formed by the combination of iron ion and hydroxide ion:

$$Fe^{2+} + 2OH^{-} \rightarrow Fe(OH)_2 \quad (2)$$

Fe $(OH)_2$ is first oxidized to form FeOOH. Then, due to the instability of FeOOH, it is oxidized to Fe_2O_3 in the presence of oxygen, as described in reactions (3) and (4):

$$2Fe(OH)_2 + \tfrac{1}{2}O_2 \rightarrow 2FeOOH + H_2O \quad (3)$$

$$2FeOOH \rightarrow Fe_2O_3 + H_2O \quad (4)$$

The cathodic reaction in neutral or alkaline medium is mainly the reduction of oxygen[34, 37]:

$$O_2 + 2H_2O + 4e^{-} \rightarrow 4OH^{-} \quad (5)$$

Comparing with Figs. 7 (a) and (b), it can be found that the passivation effect formed by immersing in ACMW for 7 d was better than that of CMW. It can be seen from Figs. 8 and 9 that with the prolongation of immersion time, the internal and edge morphology of pitting pits became more and more complex, and the perimeter area ratio became larger and larger. In addition, the passive film of stainless steel was corroded by breakdown after immersion in ACMW, and the size of pitting pit formed was larger than that formed in CMW. When stainless steel was immersed in ACMW for 4 m to 12 m, the size of pitting pit increased about 4 times. However, in the CMW, under the same immersion time, the pitting pit only increased by about 1.5 times. Although the results of the qualitative analysis can not be used to absolutely determine the properties of the developing passive film, it was obvious that these results effectively confirm the conclusions obtained from the quantitative analysis of the above potentiodynamic polarization experiment and EIS experiment.

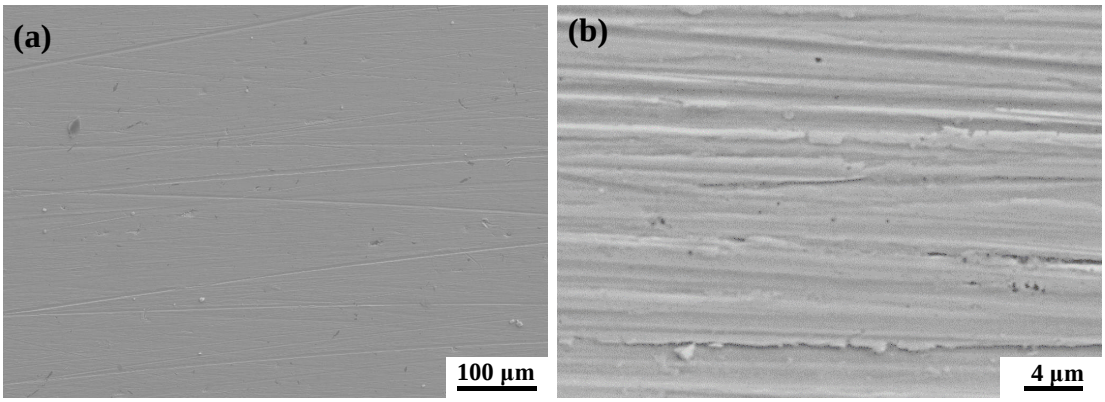

Figure 6. SEM images of the surface of experimental stainless steel at the beginning (immersion time = 0 d)

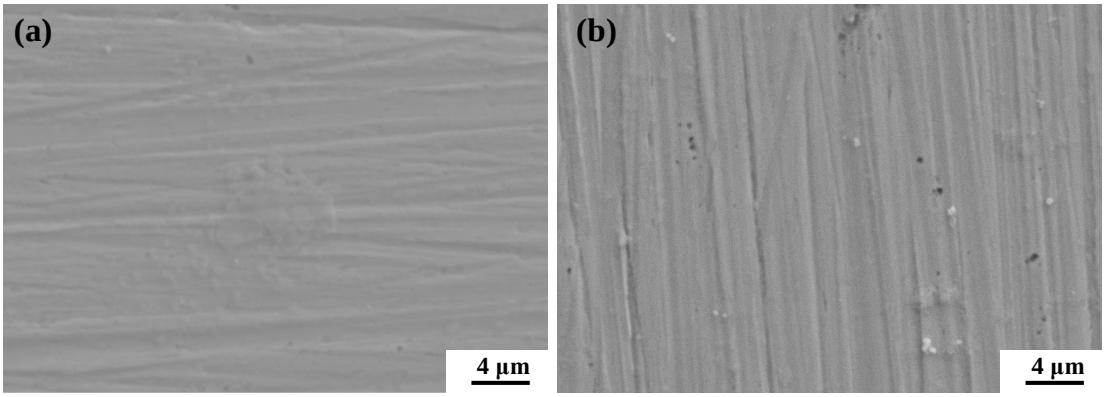

Figure 7. SEM images of the surface of experimental stainless steel after immersion in different test solutions for 7 days: (a) pH=4, (b) pH=7.

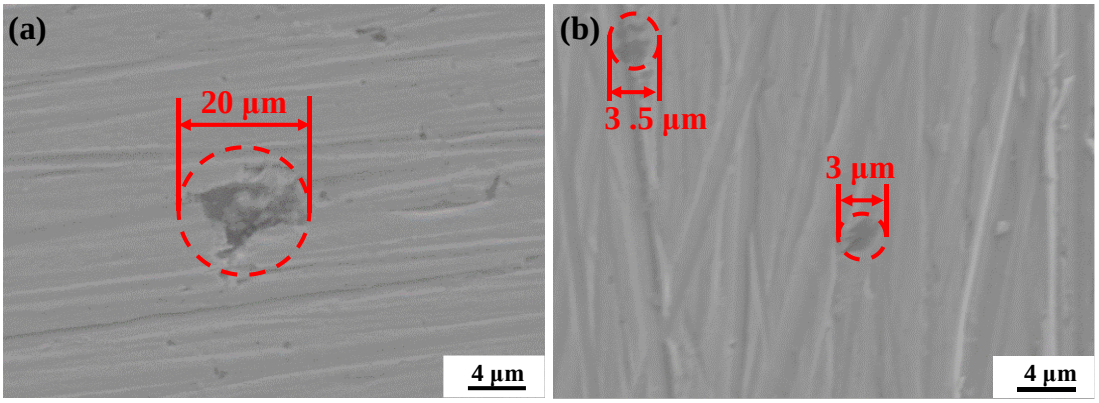

Figure 8. SEM images of the surface of experimental stainless steel after immersion in different test solutions for 4 m: (a) pH=4, (b) pH=7.

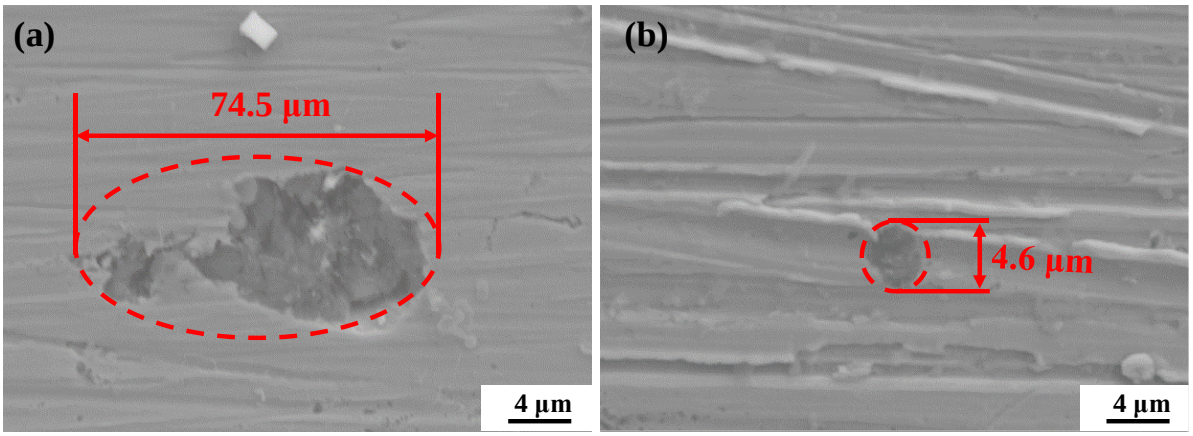

Figure 9. SEM images of the surface of experimental stainless steel after immersion in different test solutions for 12 m: (a) pH=4, (b) pH=7.

4. CONCLUSIONS

This paper presents the results of the study on the corrosion of 316L stainless steel in two kind

of coastal mine solutions with different pH. The neutral and acid pit water simulation solutions were used and electrochemical and morphological examination were carried out. According to the results, the following conclusions were drawn:

(1) According to the OCP and potentiodynamic polarization curves, the growth of passive film on 316L stainless steel surface immersed in the simulated solution of acidic coastal mine water with pH value of 4 was faster than that in the simulated solution of coastal mine water with pH value of 7. However, from the analysis of corrosion potential and pitting potential, 316L stainless steel was more easily corroded in acidic coastal mine water simulation solution with pH value of 4 than in coastal mine water with pH value of 7.

(2) 316L stainless steel was initially passivated, but pitting corrosion occurred after immersion for about 4 m. Passivation film played the role of protecting capacitor before pitting corrosion. During long-term immersion, the stable pitting was mainly controlled by the mixture of charge transfer and diffusion.

(3) The results of EIS test show that the passivation film obtained in the water medium of seaside mine with pH of 7 had better passivation performance.

(4) The results of SEM images further confirmed that for 316L stainless steel, the corrosion of acidic coastal mine water with pH value of 4 was stronger than that of coastal mine water with pH value of 7. Especially from the variation trend of pitting size, it could be seen that the growth of pitting in acidic corrosion solution from 4 m to 12 m was about 4 times, and that in neutral corrosion solution from 4 m to 12 m was about 1.5 times.

ACKNOWLEDGMENTS
This study was supported by funds from the National Natural Science Foundation of China (51774045), the National Key Research and Development Program of China (grant number 2017YFC0804604). The authors would like to thank Xincheng Gold Mine of Shandong Gold Group Co., Ltd. for providing the seashore mine solution.

References

1. Y. Zhang, H. Zhao, L. Qian, M. Sun, X. Lv, L. Zhang, J. Petersen, G. Qiu, *Miner. Eng.*, 158 (2020) 106586.
2. M. Ye, G. Li, P. Yan, J. Ren, L. Zheng, D. Han, S. Sun, S. Huang, Y. Zhong, *Chemosphere*, 185 (2017) 1189.
3. K. Wang, Y. Peng, K. Hudson-Edwards, W. Lyu, L. Bu, *Chinese J. Eng.*, 40 (2018) 526.
4. C. Falagán, B.M. Grail, D.B. Johnson, *Miner. Eng.*, 106 (2017) 71.
5. C. Lei, B. Yan, T. Chen, X. M. Xiao, *J. Clean. Prod.*, 158 (2017) 73.
6. B. Dold, *Minerals*, 4 (2014) 621.
7. L. Ma, T. Xiao, Z. Ning, Y. Liu, H. Chen, J. Peng, *Sci. Total. Environ.*, 724 (2020) 138176.
8. K. Wang, P. Yang, G. Yu, C. Yang, L. Zhu, *Water*, 12 (2020) 2538.
9. H. Luo, H. Su, B. Li, G. Ying, *Appl. Surf. Sci.*, 439 (2018) 232.
10. D. Xu, Z. Ma, S. Guo, X. Tang, Y. Guo, S. Wang, *Int. J. Hydrogen Energ.*, 42 (2017) 19819.
11. F. Arjmand, L. Zhang, J. Wang, *Nucl. Eng. Des.*, 322 (2017) 215.
12. J. Hesketh, E.J.F. Dickinson, M.L. Martin, G. Hinds, A. Turnbull, *Corros. Sci.*, 182 (2021) 109265.

13. I. Taji, S. Ghorbani, J. de Brito, V.W.Y. Tam, S. Sharifi, A. Davoodi, M. Tavakkolizadeh, *J. Clean. Prod.*, 210 (2019) 837.
14. N.T.C. Oliveira, A.C. Guastaldi, *Corros. Sci.*, 50 (2008) 938.
15. S.Y. Yu, C.W. Brodrick, M.P. Ryan, J.R. Scully, *J. Electrochem. Soc*., 146 (1999) 4429.
16. A.M. Fekry, *Electrochim. Acta*, 54 (2009) 3480.
17. S.S. Xin, M.C. Li, *Corros. Sci.*, 81 (2014) 96.
18. C. Xu, Y. Zhang, G. Cheng, W. Zhu, *Chinese J. Chem. Eng.*, 14 (2006) 829.
19. Z.B. Wang, H.X. Hu, C.B. Liu, Y.G. Zheng, *Electrochim. Acta*, 135(2014) 526.
20. M. Sánchez, J. Gregori, C. Alonso, J.J. García-Jareño, H. Takenouti, F. Vicente, *Electrochim. Acta*, 52 (2007) 7634.
21. L. Freire, M.J. Carmezim, M.G.S. Ferreira, M.F. Montemor, *Electrochim. Acta*, 55 (2010) 6174.
22. S. Arzola, J. Genescá, *J. Solid State Electr.*, 9 (2005) 197.
23. Y. Cao, S. Dong, D. Zheng, J. Wang, X. Zhang, R. Du, G. Song, C. Lin, *Corros. Sci.*, 126 (2017) 166.
24. X. Feng, R. Shi, X. Lu, Y. Xu, X. Huang, D. Chen, *Corros. Sci.*, 124 (2017) 150.
25. J. Jiang, D. Wang, H. Chu, H. Ma, Y. Liu, Y. Gao, J. Shi, W. Sun, *Materials*, 10 (2017) 412.
26. F. Tang, X. Cheng, G. Chen, R.K. Brow, J.S. Volz, M.L. Koenigstein, *Electrochim. Acta*, 92 (2013) 36.
27. C.Q. Ye, R.G. Hu, S.G. Dong, X.J. Zhang, R.Q. Hou, R.G. Du, C. Lin, J.S. Pan, *J. Electroanal. Chem.*, 688 (2013) 275.
28. M.F. Gromboni, A. Sales, M.d.A.M. Rezende, J.P. Moretti, P.G. Corradini, L.H. Mascaro, *J. Clean. Prod.*, 284 (2021) 124697.
29. G. Liu, Y. Zhang, M. Wu, R. Huang, *Constr. Build. Mater.*, 157 (2017) 357.
30. R. Liu, L. Jiang, J. Xu, C. Xiong, Z. Song, *Constr. Build. Mater.*, 56 (2014) 16.
31. Z. Ai, J. Jiang, W. Sun, D. Song, H. Ma, J. Zhang, D. Wang, *Appl. Surf. Sci.*, 389 (2016) 1126.
32. Y. Liu, Z. Song, W. Wang, L. Jiang, Y. Zhang, M. Guo, F. Song, N. Xu, *J. Clean. Prod.*, 214 (2019) 298.
33. S. Omanovic, S.G. Roscoe, *J. Colloid. Interf. Sci.*, 227 (2000) 452.
34. P.H. Refait, M. Abdelmoula, J.M.R. GÉnin, *Corros. Sci.*, 40 (1998) 1547.
35. G.A. Zhang, Y.F. Cheng, *Corros. Sci.*, 51 (2009) 901.
36. K. Xiao, C.f. Dong, X.G. Li, F.M. Wang, *J. Iron Steel Res. Int.*, 15 (2008) 42.
37. Y. Li, Z. Liu, E. Fan, Y. Huang, Y. Fan, B. Zhao, *J. Mater. Sci. Technol.*, 64 (2021) 141.
38. C. Wang, J. Chen, B. Hu, Z. Liu, C. Wang, J. Han, M. Su, Y. Li, C. Li, *J. Clean. Prod.*, 238 (2019) 117823